Journal of the European Ceramic Society **11** (1993) 363–373

Oxidation Behaviour and Mechanical Properties of β- and Mixed α–β-Sialons Sintered with Additions of Y_2O_3 and Nd_2O_3

Jeanette Persson, Thommy Ekström, Per-Olov Käll & Mats Nygren

Department of Inorganic Chemistry, Arrhenius Laboratory, Stockholm University, S-106 91, Stockholm, Sweden

(Received 10 March 1992; revised version received 3 July 1992; accepted 1 August 1992)

Abstract

Sialon ceramics have been prepared from two different Si_3N_4 powders obtained from different commercial sources, using Y_2O_3 and/or Nd_2O_3 as sintering aid. Although both powders were high-purity and high-quality silicon nitrides, surprisingly different phase compositions were obtained for the same overall starting compositions upon sintering at 1825°C. The phase compositions, densities, microstructures and mechanical properties of the samples obtained from the two powders have been compared. The samples prepared from one of the powders were oxidized at 1350°C for 20 h in dry oxygen in a TG unit. The oxidation curves obtained have been interpreted within the framework of a new rate law. The new rate law covers the observation that the oxidation behaviour of Si_3N_4-based ceramics is often non-parabolic, probably as a result of crystallization processes and the formation of cracks and/or bubbles within the oxide scale or at the scale/matrix interface during oxidation.

Sialon-Keramiken wurden aus zwei Si_3N_4-Pulvern unterschiedlicher Hersteller mit Y_2O_3 und/oder Nd_2O_3 als Sinterhilfsmittel hergestellt. Obwohl beide Si_3N_4-Pulver qualitativ hochwertig und hochrein waren, wurden nach dem Sintern bei 1825°C überraschend unterschiedliche Phasenzusammensetzungen trotz gleicher Anfangszusammensetzungen ermittelt. Die Phasenzusammensetzungen, Dichten, Mikrostrukturen und mechanischen Eigenschaften der beiden Keramiken wurden miteinander verglichen. Aus einem der beiden Pulver hergestellte Proben wurden in einer TG-Apparatur bei 1350°C während 20 h in trockenem Sauerstoff oxidiert. Die erhaltenen Oxidationskurven wurden im Rahmen eines neuen Oxidationsratengesetzes interpretiert. Es beinhaltet die Beobachtung, daß das Oxidationsverhalten von Si_3N_4-Keramiken häufig nichtparabolisch ist, was wahrscheinlich durch Kristallisationsprozesse und die Bildung von Rissen und/oder Blasen in der Oxidschicht oder an der Grenzfläche zwischen Oxidschicht und Matrix während der Oxidation verursacht wird.

Des céramiques en sialon ont été préparées à partir de deux poudres commerciales différentes de Si_3N_4, en utilisant Y_2O_3 et/ou Nd_2O_3 comme aides au frittage. Bien que les deux poudres soient de haute pureté et de qualité élevée, il est surprenant de constater que des phases différentes ont été obtenues par frittage à 1825°C, en partant d'une composition globale identique. Nous avons comparé, pour les deux poudres, les compositions cristallines, les densités, les microstructures et les propriétés mécaniques des échantillons obtenus. Ceux préparés à partir d'une des poudres ont subi une oxydation dans l'oxygène sec à 1350°C durant 20 h; l'étude a été menée par thermogravimétrie. Les courbes d'oxydation ont été interprétées sur base d'une nouvelle loi de vitesse. Cette nouvelle loi résulte de l'observation que le comportement à l'oxydation des céramiques à base de Si_3N_4 est souvent d'allure non-parabolique, probablement en raison des processus de cristallisation et de la formation de fissures et/ou de bulles dans la partie oxydée ou à l'interface partie oxydée/matrice durant l'oxydation.

1 Introduction

It is well known that pressureless sintering of dense Si_3N_4-based ceramics requires the use of a sintering aid, but also that the introduction of such an aid, owing to the formation of a liquid phase, gives rise to residual glassy and/or crystalline intergranular phase(s). As a rule, the presence of such secondary phases will have a detrimental effect on the high-temperature properties of the ceramic; for example, its strength and its resistance to oxidation will usually be more or less reduced.

In previous articles phase compositions, densities

Journal of the European Ceramic Society 0955-2219/93/$6.00

and mechanical properties of sialon ceramics, pressureless sintered or hot isostatically pressed from Si_3N_4 powders from one specific commercial source (H. C. Starck, Berlin, FRG), and with additions of Y_2O_3 and/or Nd_2O_3 used as sintering aid, have been described.[1-3] The samples in this study have the same overall composition and were prepared by pressureless sintering in the same way as those in Ref. 2 but with the use of Si_3N_4 powders from another commercial source (UBE, SN10E). The first part of the present work is devoted to a comparison of the somewhat different phase compositions, densities and mechanical properties obtained with the two different high-purity, high-quality silicon nitride powders. The main part of the paper, however, is concerned with the oxidation behaviour of the samples prepared from the latter powder (i.e. UBE). The oxidation curves obtained have been interpreted within the framework of a new rate law, briefly described later, which was derived in connection with previous studies of the oxidation behaviour of Si_2N_2O ceramics.[4]

It has been demonstrated by several workers that the oxidation behaviour of Si_3N_4 ceramics is strongly dependent on both the volume and the chemical composition of the intergranular phase(s), i.e. on the amounts and types of additives used in the sintering.[5-12] It seems generally accepted that this dependence can be attributed to the following circumstances:

(i) The intergranular phases introduced by the use of an additive usually contain nitrogen and will therefore themselves be oxidized, forming various silicate phases. As the product phases formed typically have larger specific volumes than the reactants, cracks will occur in the material if the volume expansion is sufficiently large.

(ii) The glassy phase forms a network in the ceramic, providing pathways for rapid diffusion of oxygen and of other species of importance for the oxidation kinetics.

The oxidation of Si_3N_4-related ceramics (usually recorded with a TG apparatus under isothermal conditions) is often reported to obey the parabolic rate law, which indicates that the growth of the oxide scale is diffusion-controlled. The parabolic rate law can be deduced from Fick's first law, and is often expressed in the form

$$(\Delta w/A_o)^2 = K_p t + B \qquad (1)$$

where Δw is the weight gain, A_o is the surface area of the sample, K_p is the parabolic rate constant, t is the reaction time and B is an additive constant (ideally $=0$).

Careful oxidation experiments performed at different temperatures on Si_2N_2O ceramics, and on Si_2N_2O ceramics contaminated with Ba, have recently yielded completely or partly (initial branch) non-parabolic oxidation curves.[4,13]

A model has been developed by the authors to account for the non-parabolic rate law behaviour rather frequently observed in these materials. The model is based on the assumption that deviations from the parabolic behaviour can be attributed to a decrease of the cross-sectional area for diffusion, which might occur as a result of crystallization processes, and to the formation of cracks and bubbles within the oxide scale or at the scale/matrix interface. All these phenomena are frequently observed in the oxidation of Si_3N_4 ceramics. Hence, if A_o in eqn (1) is regarded not as a constant but as a monotonously decreasing parameter, a new rate law can be derived.

Partly on the basis of experimental observations the following function has been chosen to account for the decreasing cross-sectional area:

$$A(t) = A_o[1 + (f\beta - t_o^{-1})t]/[1 + (\beta - t_o^{-1})t] \qquad (2)$$

In eqn (2) β is the constant that expresses the rate of the decrease. (The constants f and t_o are described later.) By substituting eqn (2) for A_o in the parabolic rate law, i.e. in the equation

$$dw/dt = (1/2)A_o(K_p/t)^{1/2}$$

the new rate law becomes

$$(\Delta w/A_o) = a \arctan \sqrt{(bt)} + c\sqrt{t} \qquad (3)$$

In eqn (3) a, b and c are constants. It can be shown that the parabolic rate constant K_p of eqn (1) is related to these constants by

$$K_p = (a\sqrt{b} + c)^2 \qquad (4)$$

Also, if a parabolic behaviour is observed at a later stage of the oxidation experiment (i.e. after an initial time lapse t_o, where $t_o > 0$), then one will have

$$(\Delta w/A_o)^2 = K_p^o t + B_o \qquad (5)$$

In eqn (5) K_p^o is the apparent parabolic rate constant for $t \geq t_o$ and B_o is an additive constant >0. The fraction f of the initial area, A_o, remaining at t_o can be calculated from

$$f = [a\sqrt{b}(bt_o + 1)^{-1} + c]/(a\sqrt{b} + c) \qquad (6)$$

The apparent parabolic rate constant K_p^o of eqn (5) is related to the 'true' constant K_p of eqn (1) by $f^2 K_p = K_p^o[t_o/(t_o + B_o/K_p^o)]$. It is seen from this expression that if the term B_o/K_p^o is small compared with t_o, then $f^2 K_p \approx K_p^o$.

If α denotes the growth rate of the oxide scale, then

$$\alpha = K_p/\rho_o^2 = (a\sqrt{b} + c)^2/\rho_o^2 \qquad (7)$$

In eqn (7) ρ_o represents the 'density' of the growing

oxide scale, i.e. it relates the recorded weight gain to the volume of the oxide scale (see later). Note that α has the same dimensions as a diffusion coefficient, viz. area · time^{-1}. Further, β, the rate of decrease of the cross-sectional area, is related to the constants t_0 of eqn (2) and b of eqn (3) by

$$\beta = b + t_0^{-1} \tag{8}$$

Since for a protective oxide scale the weight change of the sample can be attributed to the amount of oxygen that has been taken up by and the amount of nitrogen that has been released from the sample, the 'density', ρ_0, is defined by

$$\rho_0 = (32{\cdot}00n_O - 28{\cdot}02n_N)/\sum(n_i M_i/\rho_i) \tag{9}$$

where n_O = number of moles of O_2(g) absorbed by the sample, n_N = number of moles of N_2(g) released from the sample, n_i = number of moles of the solid product phase i, M_i = the formula weight of the product phase i and ρ_i = the density of the product phase i. The relationship between n_O, n_N and n_i is then determined by the overall reaction equation for the oxidation. (ρ_0 is a 'density' only in the formal sense that it is defined by dividing weight by volume.)

A detailed derivation of this model has been given in Ref. 4. Although the interpretation of the oxidation of Si_2N_2O ceramics with the use of the new model has yielded surprisingly consistent results, it still remains to be shown whether the model can be applied to more complicated systems like those discussed in this article.

2 Experimental

The overall compositions of the samples selected for this study are shown in Fig. 1. Of these samples, A is a β-sialon with a weighed-in z value of about 0·95, where z is defined by the formula $Si_{6-z}Al_zO_zN_{8-z}$, with $0 \leq z \leq 4$. B and C are mixed α–β-sialons, where C has a higher content of α-sialon phase than B. The α-sialon phase can be described by $Me_x(Si,Al)_{12}(O,N)_{16}$, where, in this case, Me = Y and Nd.

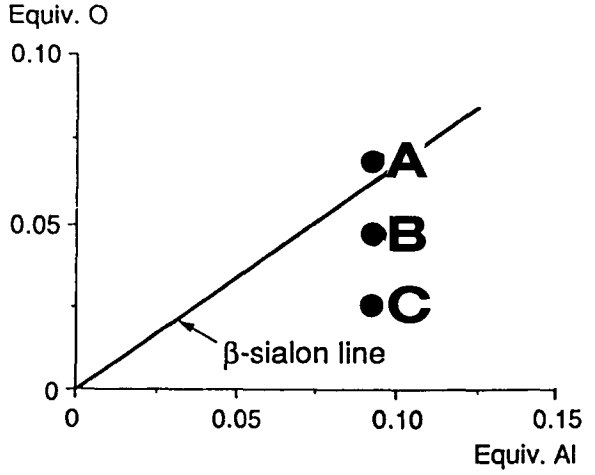

Fig. 1. The overall composition of the samples selected for this study. A is a β-sialon, and B and C are mixed α–β-sialons. (Note that the oxygen present in the Y_2O_3 and Nd_2O_3 additives has not been included in the calculation of the oxygen equivalents.)

Each of the compositions in Fig. 1 was prepared with three different additions of Y_2O_3/Nd_2O_3, viz. 100/0, 50/50 and 0/100. The corresponding samples will in the following be denoted $X1$, $X2$ and $X3$ (X = A, B, C). The same constant molar amount of Y_2O_3/Nd_2O_3 was added to all samples, corresponding to 6·0 wt% for the pure yttria ($X1$) and 8·9 wt% for the pure neodymia ($X3$) additions.

The green powder mixtures in this study were prepared from Si_3N_4 (UBE, SN10E), Al_2O_3 (Alcoa, A16SG), AlN (H. C. Starck, Berlin, grade A), Y_2O_3 (H. C. Starck, Berlin, 99·9%) and Nd_2O_3 (Molycorp. Inc., >99·5%). In calculating the compositions, corrections were made for the small amounts of oxygen present in the Si_3N_4 and AlN raw materials. In previous studies on Y/Nd-sialons, silicon nitride from H. C. Starck (Berlin, grade LC1) was used.[2]

Pressed tablets of the powders were fired at 1825°C for 2 h in nitrogen. The densities of the sintered specimens were measured by Archimedes' principle in toluene and in water. The hardness (HV10) and indentation fracture toughness (K_{IC}) at room temperature were obtained with a Vickers diamond indenter with a 10-kg load. The K_{IC} values were determined according to the method of Anstis *et al.*,[14] assuming a value of 300 GPa for Young's modulus.

The crystalline phases formed were identified from X-ray diffraction patterns recorded in a Guinier–Hägg camera with CuK_{α_1} radiation and Si as internal standard. The crystalline phases present in the oxide scales were identified with an X-ray powder diffractometer (STOE STADI) operated in reflection mode and using CuK_{α_1} radiation. Cross-sections of the oxide scales were studied in SEM (Jeol 820 and 880) equipped with energy-dispersive spectrometers (Link AN 10000).

The oxidation experiments were performed in a TG unit (SETARAM TAG 24), provided with two symmetric furnaces; one used for the oxidation of the sample and the other for reference. The resolution of the TG unit is better than 2 μg, and the baseline drift during a 20-h experiment can be kept within ±5 μg by precise regulation of the gas flow. Sialon pieces of the approximate size 15 × 15 × 1 mm^3 were oxidized at 1350°C for 20 h in flowing, dry oxygen. Prior to the oxidation, the ceramic specimens were carefully polished with diamond paste (grains down to a size <1 μm) and cleaned in an ultrasonic bath.

3 Results and Discussion

3.1 Density and phase analysis

As already mentioned, the Si_3N_4 powder used for the preparation of the samples in this study was from UBE. The Starck powder, however, was used in previous studies of β- and mixed α–β-sialons, and it was found that with respect to phase composition the two powders yielded significantly different results for the same overall starting compositions. A comparison of the two powders will therefore be made.

The densities, expressed as percentages of the theoretical densities, of the samples prepared from the Starck and the UBE powders at 1825°C are listed in Table 1, and the observed crystalline phases of the corresponding samples are given in Table 2. Included in the latter table are also the observed z values of the β-sialon $Si_{6-z}Al_zO_zN_{8-z}$, the estimated α/β ratios of the mixed α–β-sialons and a rough estimate of the intergranular phase volumes. The z values and the α/β ratios were calculated according to expressions given in Refs 15 and 16, and the volume of intergranular phase from SEM micrographs.

The small density differences, for the A and B compositions, between the samples prepared from the UBE and the Starck powders (Table 1) may not be significant; they could well be due to the way in which the theoretical densities were determined.[2] However, while all the Starck powder samples were fully or almost fully dense at 1825°C, this was not the case for the UBE (at least not for the C) samples. In particular, the densification of sample C3 was very poor. A possible explanation for this is that a substantial incorporation of the sintering additive into the α-sialon phase reduces the available amount of liquid phase during sintering. In addition, for stoichiometric reasons, the intergranular phase of the C samples will be enriched in nitrogen and will thus be more viscous.

Table 1. Observed densities, expressed as percentages of the theoretical densities, of β- and mixed α–β-sialons prepared from two different Si_3N_4 powders

Sample[a]	Y_2O_3/Nd_2O_3	*1825°C*[b]	*1825°C*[c]
A1	100/0	100	99·0
A2	50/50	100	98·1
A3	0/100	100	99·9
B1	100/0	100	98·9
B2	50/50	100	99·6
B3	0/100	100	—
C1	100/0	99·5	97·1
C2	50/50	99·0	96·7
C3	0/100	98·2	79·8

[a] The samples were sintered at 1825°C.
[b] H. C. Starck, Berlin, LC1.
[c] UBE, SN10E.

It is seen in Table 1 that for the samples which did not attain full density, the density tended to decrease with decreasing Y_2O_3/Nd_2O_3 ratio. In other words, as was shown in previous work, Y_2O_3 is a better aid than Nd_2O_3 in pressureless sintering.

It is clear from Table 2 that the UBE powder yielded much higher α/β ratios than the Starck powder. In fact, even the pure β-sialon compositions contained some α-sialon phase when prepared from the UBE powder. It can be noted that only small amounts of Nd-melilite ($Nd_2Si_{3-x}Al_xO_{3+x}N_{4-x}$, $x \approx 0{\cdot}9$) were found in sample C3 prepared from the UBE powder, whereas appreciable amounts were found in the corresponding sample prepared from the Starck powder. Again, this is consistent with an expected lower amount of Nd available in the intergranular phase for melilite formation in the UBE sample.

The observed unit cell dimensions of the α-sialon

Table 2. Observed phases in β- and mixed α–β-sialon samples prepared from two different Si_3N_4 powders

Sample	Y_2O_3/Nd_2O_3	*1825°C*[b]				*1825°C*[c]			
		Intergranular phases[d]	*Volume*[a] *(%)*	$\alpha/(\alpha+\beta)$	z[e]	*Intergranular phases*[d]	*Volume*[a] *(%)*	$\alpha/(\alpha+\beta)$	z[e]
A1	100/0	B w	~8	—	0·66	B w	~9	0·08	0·65
A2	50/50	—	—	—	0·67	—	—	0·06	0·63
A3	0/100	M	~20	—	0·65	M	~15	0·04	0·58
B1	100/0	B	~6	0·40	0·63	B	~11	0·47	0·48
B2	50/50	—	—	0·30	0·63	—	~6	0·45	0·50
B3	0/100	M	~16	0·10	0·54	M	~9	0·22	0·51
C1	100/0	B vw	~6	0·58	0·54	—	—	0·91	~0·5
C2	50/50	—	—	0·55	0·52	M w	~4	0·83	~0·5
C3	0/100	M	~16	0·33	0·44	M w	~5	0·75	0·27

[a] The intergranular phase volumes were estimated from SEM micrographs.
[b] H. C. Starck, Berlin, LC1.
[c] UBE, SN10E.
[d] M = Nd-melilite; B = B-phase (Y_2SiAlO_5N); w = weak.
[e] z value of the β-sialon solid solution, $Si_{6-z}Al_zO_zN_{8-z}$.

phase were $a = 7{\cdot}802(5)$ and $c = 5{\cdot}680(3)$ Å, regardless of the overall composition and type of powder used. This indicates that all α–β compositions selected for this study were in 'equilibrium' with an α-phase composition identical or very close to the lower end of the α-sialon substitution range.[17]

Concerning the chemical differences between the UBE and the Starck powders, it can be noted that the oxygen contents of the two powders are roughly equal (1·3–1·5 wt%) but that the amount of other impurities is lower in the UBE powder. For example, the UBE powder contains no carbon or halides, whereas these impurities in the Starck powder amount to about 0·5 wt%. However, the kinetic reasons for the high α-sialon yield of the UBE powder compared with that of the Starck powder are not clear.

From the data in Table 2 the following three tendencies can be extracted:

(i) For the mixed α–β-sialons the α/β ratio decreases with increasing Nd content.

(ii) The amount of intergranular phase increases with increasing Nd content. This tendency seems clear for most samples except for the B samples prepared from the UBE powder, which show a slight trend to the contrary. This 'anomaly', however, might well be attributed to the rather low accuracy in the estimated intergranular phase volumes. As one would expect, the C samples generally appear to contain smaller volumes of intergranular phase than do the A and B samples.

(iii) At least for the samples prepared from the Starck powder there is a small but probably significant decrease of the z values with increasing Nd content in mixed α–β-sialons. Also, all observed z values of the β-sialons are less than the weighed-in value (~0·95), indicating that some aluminium has been used up in the formation of the intergranular phase(s).

3.2 Microstructure

The microstructures of the samples prepared from the Starck powder have been described in detail in previous work.[1–3] The microstructures of the samples prepared from the UBE powder have a similar appearance, except for the differences in phase amounts already described and a slightly finer overall grain size.

The compositions of the α-sialon phase, as determined by EDS analysis, in the samples C1, C2 and C3 (sintered from the Starck powder) were, respectively,

$$Y_{0{\cdot}42}Si_{10{\cdot}3}Al_{1{\cdot}7}O_{0{\cdot}40}N_{15{\cdot}6}$$

$$Y_{0{\cdot}21}Nd_{0{\cdot}15}Si_{10{\cdot}3}Al_{1{\cdot}7}O_{0{\cdot}63}N_{15{\cdot}4}$$

and $$Nd_{0{\cdot}33}Si_{10{\cdot}5}Al_{1{\cdot}5}O_{0{\cdot}53}N_{15{\cdot}5}$$

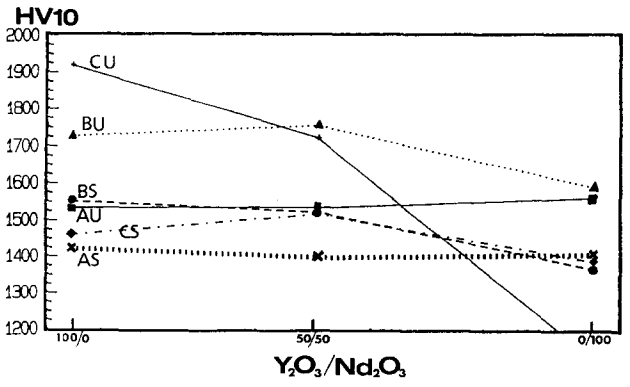

Fig. 2. The variation in measured Vickers hardness (load 98 N, HV10 scale) when Y_2O_3 is replaced by Nd_2O_3 as sintering aid. *X*S and *X*U denote samples prepared from the Starck and the UBE powders, respectively, where *X* = sample A, B, C.

These compositions are in agreement with the observed cell parameters of the α-sialon phase. The compositions also support the notion that the smaller Y^{3+} enters more easily into the α-sialon structure than the larger Nd^{3+}, and also explain the higher α/β ratios observed when Y is used (cf. Table 2).

3.3 Physical properties

The results of the hardness (HV10) and fracture toughness (K_{IC}) measurements are compiled in Figs 2 and 3, respectively. It is interesting that the samples prepared from the UBE powder in general have both higher hardness and fracture toughness than the samples prepared from the Starck powder. It is also noteworthy that sample C1, prepared from the UBE powder and with an α/β ratio of about 90%, not only is much harder than any other sample (HV10 = 1918) but also has the highest fracture toughness ($K_{IC} = 5{\cdot}11$) of all samples sintered with pure Y_2O_3. As will be shown, this sample also exhibited the best oxidation resistance of all.

For all samples a drop in the hardness is observed when yttria is replaced by neodymia as sintering aid, while the fracture toughness essentially remains the same or perhaps increases a little. However, the

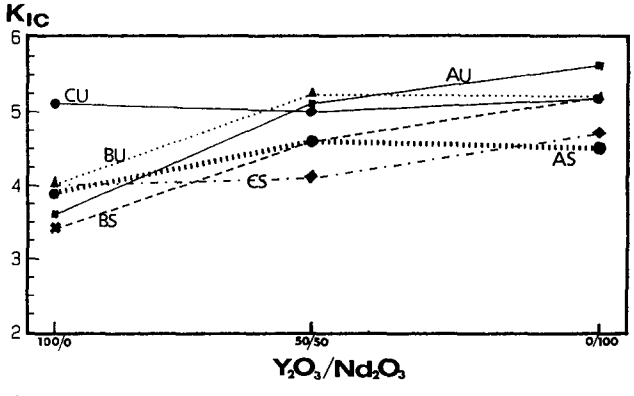

Fig. 3. The variation in measured indentation fracture toughness (K_{IC}) when Y_2O_3 is replaced by Nd_2O_3 as sintering aid. *X*S and *X*U denote samples prepared from the Starck and the UBE powders, respectively, where *X* = sample A, B, C.

dramatic drop in hardness for sample C3 prepared from the UBE powder (Fig. 2) is believed to be due to the high porosity of that sample (~80% TD).

It is well established that α-Si_3N_4 is harder than β-Si_3N_4.[18] Conversely, owing to the elongated form of the β-crystals, β-Si_3N_4 (or β-sialon) ceramics generally have a higher fracture toughness than α-Si_3N_4 (or α-sialon) ceramics.[19] According to the above phase analysis, the decrease in hardness of the neodymia-rich samples can be attributed to two sources: the increased amount of 'soft' intergranular phase (HV10 ~900–1000) at all compositions and the smaller amount of hard α-phase in mixed α–β-sialon samples. The high hardness of the mixed Y-doped α–β-sialons prepared from the UBE powder is mainly a consequence of the high α-phase content of these samples.

The high-temperature mechanical properties of silicon nitride ceramics prepared from different sources of Si_3N_4 powders have previously been evaluated.[20,21] It was found that the UBE powder gave materials with better high-temperature properties than the Starck powder, and it was concluded that the failure of the latter material was not primarily related to differences in oxygen content between the powders but to other impurities or contaminants.

3.4 Oxidation behaviour

3.4.1 TG curves

All samples used in the oxidation experiments were prepared from the UBE powder, which, as already described, yields much higher α/β ratios for mixed α–β-sialon compositions than the Starck powder. In general, the intergranular phase volumes also appeared to be smaller in the samples prepared from the UBE powder than in those obtained from the Starck powder (Table 2).

The oxidation curves for all sialon samples are shown in Fig. 4. All oxidation experiments were carried out isothermally at 1350°C. The oxidation curves for the A samples are shown in Fig. 4(a), and those of the B and C samples in Fig. 4(b) and (c), respectively. Two tendencies can be clearly distinguished from these curves. Firstly, the oxidation resistance increases with increasing α/β ratio. Thus, the composition showing the best behaviour is C1, with the largest amount of α-sialon and the smallest amount of intergranular phase. Secondly, the oxidation resistance decreases when neodymia is substituted for yttria. Consequently, the sample displaying the poorest behaviour of all is A3, a β-sialon sintered with Nd_2O_3.

It is believed that, qualitatively, the above tendencies can be ascribed partly to the varying volumes of intergranular phase(s) present in the sialons and partly to compositional effects due to

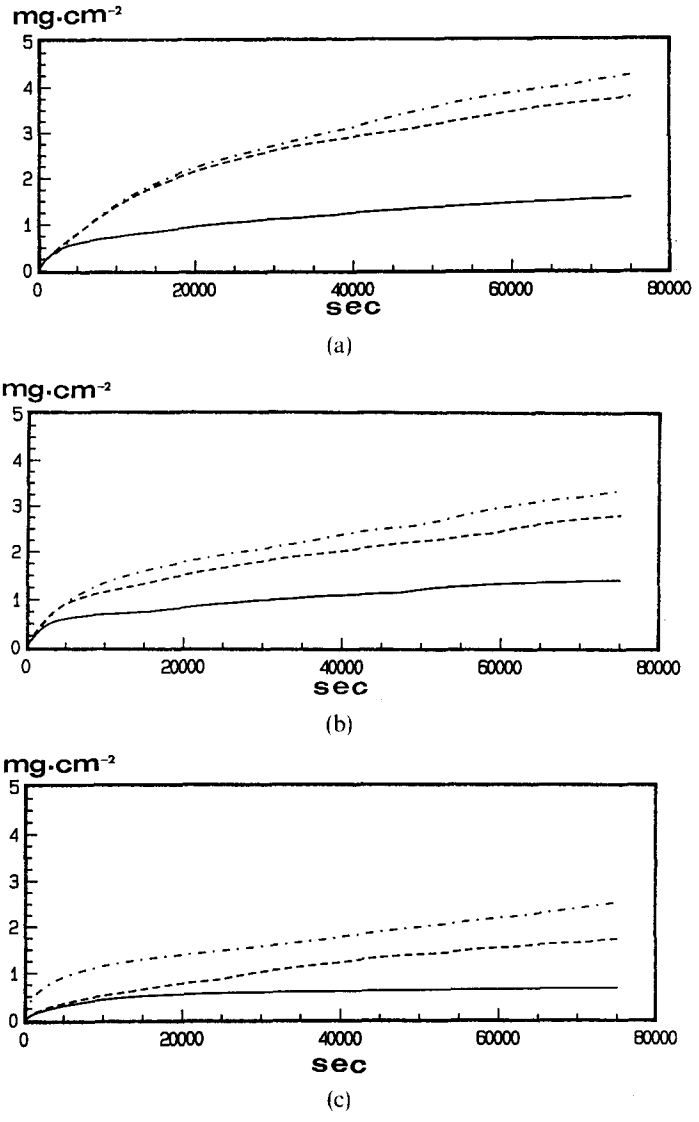

Fig. 4. Oxidation behaviour of pressureless sintered β- and mixed α–β-sialons at 1350°C, when Y_2O_3 is replaced by Nd_2O_3 as sintering aid. All samples were prepared from the UBE powder. (a) The β-sialon samples (——) A1, (– – –) A2, (– · –) A3; (b) the mixed α–β-sialon samples (——) B1, (– – –) B2, (– · –) B3; and (c) the mixed α–β-sialon samples (——) C1, (– – –) C2, (– · –) C3. The latter samples had very high contents of α-phase (Table 2).

varying Y_2O_3/Nd_2O_3 ratios. The former relationship can be illustrated by the following series. Of the pure Nd samples (i.e. A3, B3 and C3), A3 showed the poorest oxidation behaviour of all. B3 showed a somewhat better behaviour, and C3 was still better. The estimated relative volumes of intergranular phase of A3, B3 and C3 were 15%, 9% and 5%, respectively, and the estimated contents of α-phase for the same samples were 4%, 23% and 75% (see Table 2). Accordingly, a relationship seems to exist between the amount of intergranular phase and the oxidation behaviour, as would be expected. However, such a relationship does not imply that the volume is the only crucial factor, because when moving from a pure β-sialon to an α-sialon the composition of the intergranular phase will probably change as well. Thus, in sample C3 a substantial

amount of Nd is incorporated into the α-sialon phase, implying that the concentration of Nd in the intergranular phase might be lower in C3 than in A3. The higher overall N-content of the C samples also implies that the glass phase in C3 has a higher viscosity than that in A3.

The importance of the intergranular phase composition for the oxidation behaviour is obvious from the fact that the three samples prepared with pure yttria (A1, B1 and C1) had a better oxidation resistance than all other samples. As already shown, the volume of intergranular phase decreases when yttria alone is used as sintering aid. It is unlikely that the decrease in volume of the intergranular phase alone can account for the much better oxidation behaviour of the yttria samples. For example, sample A1, with an estimated glass content of ~9% and only small amounts of α-phase (8%), showed a better oxidation behaviour than C2 and C3, both of which appeared to have smaller volumes of intergranular phase (4% and 5%, respectively) and much larger contents of α-phase (83% and 75%, respectively) than A1. Another factor which can be expected to influence the oxidation resistance is the viscosity of the intergranular glass. Considering the higher viscosity of an YSiAlON glass compared with the Nd-containing glasses, one would also expect the A1, B1 and C1 samples to exhibit the best oxidation resistance. As to the oxidation behaviour, the conclusion anyhow is that Y_2O_3 rather than Nd_2O_3 should be used as sintering aid.

A similar conclusion has previously been reported by Mieskowski & Sanders,[22] who investigated the oxidation behaviour of Si_3N_4 sintered with additions of Y_2O_3, La_2O_3, Sm_2O_3 and CeO_2. The authors found the oxidation rate to be lowest with yttria.

3.4.2 Oxide scale

The SEM micrographs of the oxidized surfaces of samples A1 to A3 are shown in Fig. 5. The rather irregularly shaped 'white' crystals in Fig. 5(a) are $Y_2Si_2O_7$, and the smaller, needle-shaped crystals of a lower contrast are mullite, $3Al_2O_3 . 2SiO_2$. Between the disilicate and the mullite crystals there is a rather dark region containing crystals of α-cristobalite surrounded by glass. The low contrast yielded by the glass indicates that it contained very little Y^{3+}, if any, i.e. practically all yttrium in the oxide scale had been used up in the formation of $Y_2Si_2O_7$. Also, the crystalline phases visible in Fig. 5(a) were the only ones detected by X-ray diffraction. The oxidation of sample C1 will be discussed in some detail later. The oxide surface of this sample (and of sample B1) had a quite similar appearance to that of A1.

The appearances of the oxide surfaces of the samples A2 and A3 are similar to each other (Fig. 5(b) and (c), respectively) but different from that of A1. In A2 and A3 no disilicate phase was detected. The surfaces of these samples appear to consist of 'islands' of cristobalite and mullite in an Y/Nd-rich glass. Again, the surfaces of the samples B2 and C2, and B3 and C3, resembled those of A2 and A3, respectively.

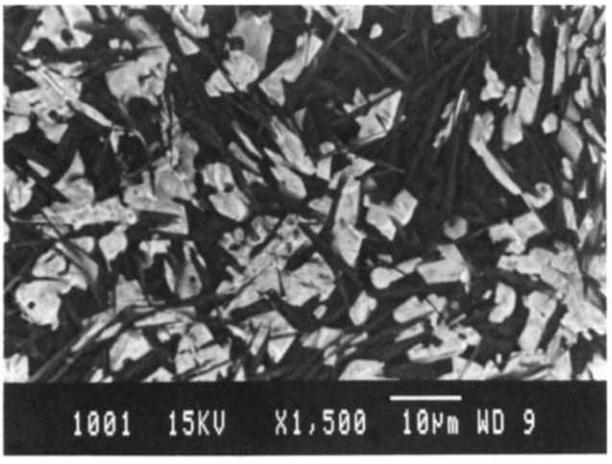

(a)

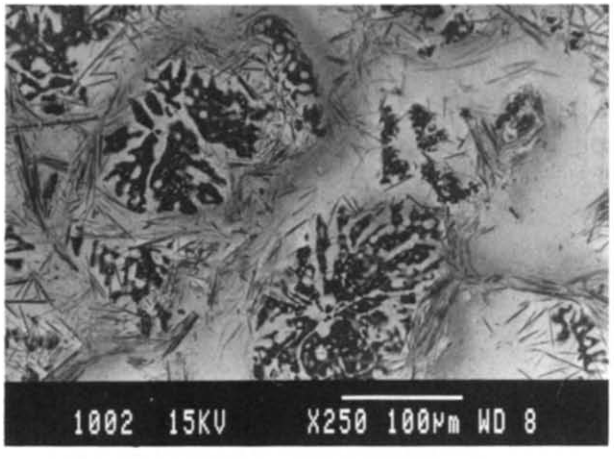

(b)

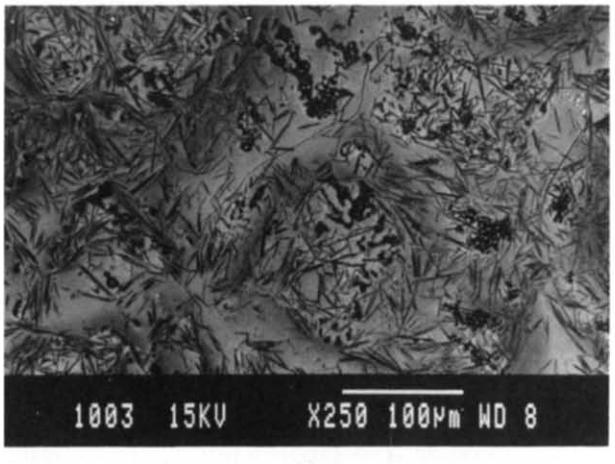

(c)

Fig. 5. SEM micrographs of the oxidized surfaces of the β-sialon samples (a) A1, (b) A2, (c) A3. The irregularly shaped 'white' crystals are $Y_2Si_2O_7$, and the smaller, needle-shaped crystals of a dark contrast are mullite, $3Al_2O_3 . 2SiO_2$. Between the disilicate and mullite crystals, crystals of cristobalite surrounded by a glass can be seen. The only observed crystalline phases in A2 and A3 were cristobalite and mullite.

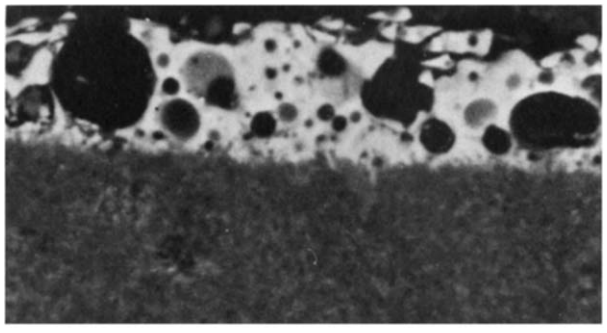

Fig. 6. Cross-section of the oxide scale of sample B3, a mixed α–β-sialon sintered with 9 wt% Nd_2O_3. Large bubbles, probably nitrogen-containing, have formed in the scale during oxidation. It is likely that the bursting of such bubbles will cause sudden increases in oxidation rate if the sub-scale ceramic is exposed to the oxidizing atmosphere. Magnification 850×.

The cross-sections of the oxide scales generally exhibited a markedly uneven character with rather ill-defined thickness and with the outer surfaces appearing fragile and sometimes ragged. The latter phenomenon might be attributed to the bursting of large nitrogen bubbles, as shown in Fig. 6.

The cross-section of the scale of sample B3 is shown in Fig. 7(a). The structure of this scale seems typical for most samples. The oxide layer, which is about 150 μm thick, consists roughly of three zones:

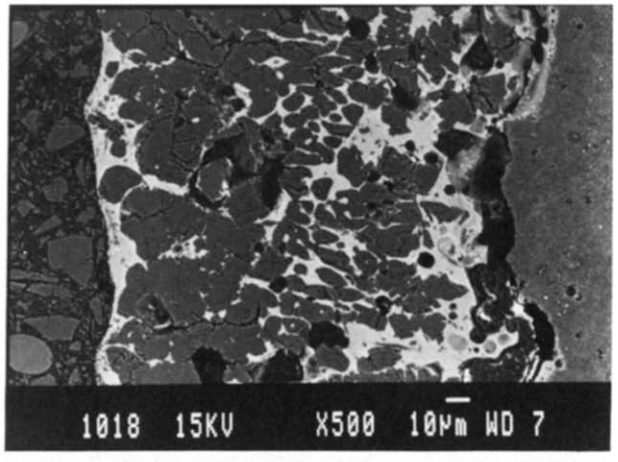

(a)

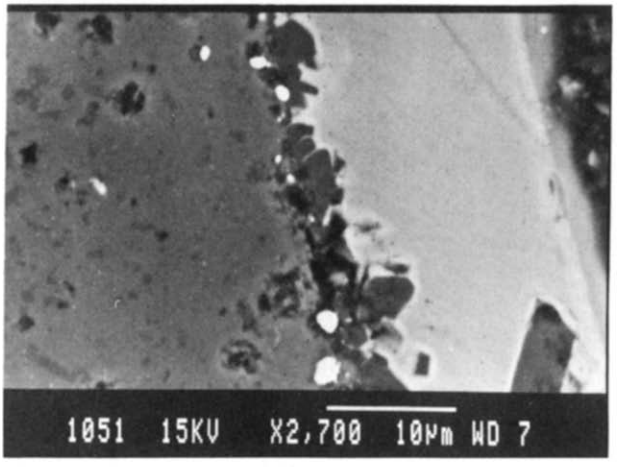

(b)

Fig. 7. Cross-sections of the oxide scales of samples (a) B3 and (b) C2.

(i) two zones with relatively large concentrations of Y^{3+} and/or Nd^{3+} ions positioned immediately below the outer surface and immediately above the scale/matrix boundary (bright areas); (ii) one broader zone, mainly occupied by cristobalite crystals (grey areas). Between the scale and the matrix a crack zone is usually observed. Probably these cracks have been caused by the cooling of the samples, and/or by the subsequent preparation of the cross-sections.

However, the micrographs of the cross-sections of samples C2 and C3 differ in appearance to sample B3 in that they exhibit outer oxide scales consisting of a rather thick (~10 μm) glass, as shown in Fig. 7(b). For the C2 sample, the glass layer appears to be smooth and homogeneous, whereas in sample C3 it contains many bubbles, most probably of nitrogen. The 'frozen-in' bubbles seem to indicate that this Nd-containing glass had a higher viscosity than the Y/Nd glasses, as might be expected.

3.4.3 Depleted zone

The presence of a rather broad zone depleted of heavy metal ions below the scale in all samples indicates that a net diffusion of both Y^{3+} and Nd^{3+} from the grain boundaries into the scale took place during the oxidation. Such a zone is shown in Fig. 8. In this micrograph, obtained from sample B3, the depleted area is shown to the left, separated from the matrix to the right by a surprisingly distinct dividing line.

The compositions of the surface glasses in samples *X*2 and *X*3 (*X* = A, B, C), as determined by EDS analysis, are listed in Table 3. In calculating these compositions it was assumed that no nitrogen could be present at the surface. (The compositions of the surface glasses in samples A1, B1 and C1 could not be reliably determined, as the glass volumes in these samples either were too small or yielded too low contrast to be identified with any certainty in SEM.)

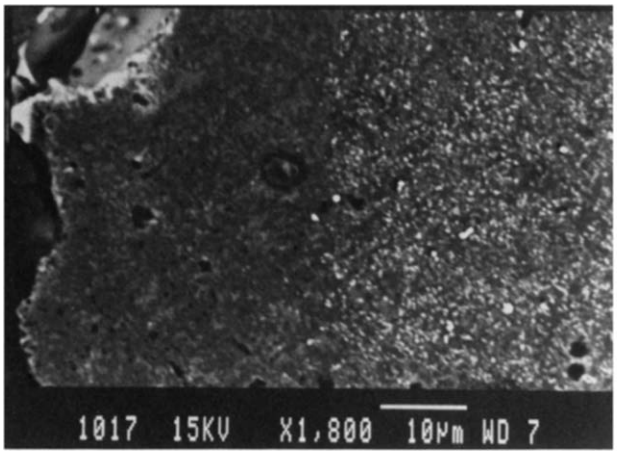

Fig. 8. A cross-section of the oxide scale of sample B3, showing the depleted zone. The depleted area (to the left) is separated from the matrix (to the right) by a distinct boundary.

Table 3. The compositions of the surface glasses in the samples *X*2 and *X*3, as determined by EDS analysis (*X* = A, B, C)

A2	$Y_{0.11}Nd_{0.07}Si_{2.0}Al_{0.93}O_{5.7}$	B2	$Y_{0.11}Nd_{0.06}Si_{1.9}Al_{1.0}O_{5.6}$	C2	$Y_{0.17}Nd_{0.22}Si_{1.4}Al_{0.56}O_{4.2}$
A3	$Nd_{0.09}Si_{2.2}Al_{0.96}O_{6.0}$	B3	$Nd_{0.10}Si_{2.1}Al_{0.96}O_{5.8}$	C3	$Nd_{0.32}Si_{1.4}Al_{0.52}O_{4.1}$

It is seen in Table 3 that the glass compositions of B2 and B3 are almost identical with the compositions of A2 and A3. On the other hand, the compositions of the surface glasses in C2 and C3 are clearly different, so that the (Y+ Nd):(Si + Al) ratio is significantly larger for C2 than for A2 and B2; and, similarly, the Nd:(Si + Al) ratio is larger for C3 than for A3 and B3. The reason for the difference in glass composition between the C2 and C3 samples on the one hand, and the A2 and B2 and A3 and B3 samples on the other, is not clear. However, the high α/β ratios of the C samples imply that substantial amounts of Y and/or Nd are used up in the formation of the α-sialon phase in these samples. Thus, the volumes and probably also the compositions of the intergranular phases in the C samples will be different from those in the A and B samples. As Al, Y and Nd from the depleted zone will contribute to the glass composition of the oxide scale, it is likely that the composition of the latter as well as the width of the depleted zone will modify the composition of the surface glass.

3.4.4 Oxidation kinetics

Most of the oxidation curves obtained from the sialon samples were not sufficiently smooth to allow unambiguous judgements about the oxidation kinetics according to eqns (1), (3) and (5). For two of the samples, B1 and C3, it was definitely impossible to determine the kinetics because of the uneven character of the curves; and for two others (A3 and B3) only the first parts of the curves could be used.

It seems likely (see Fig. 6) that the observed sudden increases in oxidation rates in those curves are due to bursting nitrogen bubbles. When such a bubble bursts through the surface, a pit is probably created in the surface layer, exposing the interior of the ceramic to the oxidizing atmosphere for a longer or a shorter time.

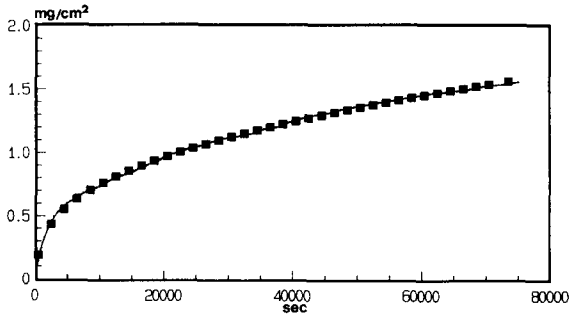

Fig. 9. The oxidation curve of sample A1, a β-sialon sintered with 6 wt% Y_2O_3. Together with experimentally observed curve (——) the fitted rate law of eqn (3) is shown (■). For the values of the constants *a*, *b*, *c* of the arctan function, see text.

In no case could a whole curve be unambiguously described as parabolic, although in most cases the later parts of the curves appeared parabolic. However, in one case, sample A1, the arctan function (eqn (3)) could account for the entire curve, and no parabolic part was observed. The curve is shown together with the fitted arctan function in Fig. 9. The calculated K_p value of this sample is $1{\cdot}41 \times 10^{-4}$ mg^2 cm^{-4} s^{-1} (eqn (4)), and the fraction *f*, as estimated from eqn (6) assuming that $t_0 = \infty$, is 0·35. As the 'density', ρ_0, of the growing oxide scale could be estimated to be about 480 mg cm^{-3} (see below), the value of the growth rate of the oxide scale, α, becomes $6{\cdot}1 \times 10^{-10}$ cm^2 s^{-1} (eqn (7)).

Sample C1 exhibited by far the best oxidation behaviour of all, and the oxidation curve was perfectly smooth. For this curve a t_0 of about 25 000 s was determined, so that for $t > t_0$ the curve seemed perfectly parabolic. However, for $t < t_0$ it was not possible to fit the arctan function (eqn (3)). Instead, the following special solution was found to fit very well to that part of the curve. This solution occurs if $\beta = t_0^{-1}$ (i.e. if *b* in eqn (3) = 0), and has the form

$$(\Delta w/A_0) = At^{1/2} + Bt^{3/2} \qquad (10)$$

Since it can be shown that $K_p = A^2$, the parabolic rate constant for this curve is $2{\cdot}91 \times 10^{-5}$ mg^2 cm^{-4} s^{-1}. The apparent rate constant K_p^o for the parabolic part of the curve is $2{\cdot}46 \times 10^{-6}$ mg^2 cm^{-4} s^{-1} (eqn (5)). The *f* value, as calculated by eqn (6), is 0·13, and $\beta = t_0^{-1} \approx 4 \times 10^{-5}$ s^{-1}. The oxidation curve for C1 together with the fitted equations, eqns (5) and (10), are shown in Fig. 10.

To estimate ρ_0 of the oxide scale of C1, it was assumed that the only solid product phases formed were cristobalite, mullite and yttrium disilicate. (It can be noted that cristobalite and amorphous SiO_2

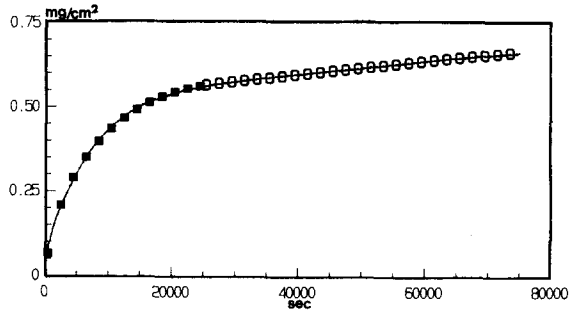

Fig. 10. The oxidation curve of sample C1, a mixed α–β-sialon sintered with 6 wt% Y_2O_3 and containing approximately 90% of α-phase (Table 2). Together with experimentally observed curve (——) the fitted rate laws of eqns (5) (○) and (10) (■) are shown. For the values of the constants K_p^o and B_0 of eqn (5) and *A*, *B* of eqn (10), see text.

have very similar densities.) The weighed-in composition of sample C1 was $Y_{0.076}Si_{2.73}Al_{0.357}O_{0.484}N_{3.75}$, yielding the approximate reaction equation

$$'Y_{0.076}Si_{2.73}Al_{0.357}O_{0.484}N_{3.75}' + 2.81O_2(g) \rightarrow 0.038Y_2Si_2O_7 + 0.06(3Al_2O_3 . 2SiO_2) + 2.53SiO_2 + 1.87N_2(g)$$

The 'density' for this reaction, as calculated from eqn (9) using the densities for cristobalite, mullite and yttrium disilicate in the denominator, is 480 mg cm^{-3}, yielding a thickness of the oxide layer (10 μm) in good agreement with the thickness observed by SEM (5–20 μm). Hence, for C1 the rate constant α becomes 1.3×10^{-10} $cm^2 s^{-1}$ (eqn (7)). The K_p value of C1 is about 1/5 of that of A1, which agrees with the better oxidation resistance of the former sample (Table 4).

According to the above model, it makes a difference whether a K_p or a K_p^o value is used, since by definition $K_p^o < K_p$. The K_p values for A1 and C1 can be compared with the parabolic rate constants reported in the literature for the oxidation in the temperature range 1300–1400°C of hot-pressed or pressureless sintered β-sialons and Si_3N_4 ceramics containing various sintering additives. The reported constants are in the range 8×10^{-6}–4×10^{-3} mg^2 $cm^{-4} s^{-1}$.[23–25] The K_p values for A1 and C1 thus are within this range. The calculated K_p and f values for the sialon samples are listed in Table 4. It should be stressed, however, that these values are uncertain owing to the difficulties already discussed.

The α value for sample C1 can be compared with the value recently obtained for pure Si_2N_2O oxidized at 1350°C, which is 2.9×10^{-12} $cm^2 s^{-1}$.[4] Considering the appreciable differences in chemistry between a mixed α–β-sialon ceramic, sintered with 6.0 wt% Y_2O_3, and an essentially single-phase Si_2N_2O ceramic, made by HIPping and where no additives were used, a factor of 45 between the two rate constants does not appear extremely large.

The obtained α values can also be compared with measured diffusion coefficients for oxygen in various silica glasses at 1350°C, as determined by ion-exchange methods. Muehlenbachs & Schaeffer reported for pure SiO_2 glass at that temperature a D_O value of 1.0×10^{-13} $cm^2 s^{-1}$.[26] For network oxygen diffusion in multicomponent silica glasses, i.e. SiO_2 with additions of Na_2O, CaO, Al_2O_3, etc., the reported D_O values are much larger: 7.8×10^{-8}–8.9×10^{-7} $cm^2 s^{-1}$ depending on the glass composition.[27] The addition of these compounds thus increases the oxygen diffusion rate by a factor of 10^5–10^6.

The α values obtained for samples A1, C1 and pure Si_2N_2O fall between the lower and upper limits of the D_O values obtained. The α value for the oxidation of single-phase Si_2N_2O is about 30 times larger than D_O for pure silica glass, and the values for A1 and C1 are 10^2–6×10^3 times less than the D_O values reported for SiO_2 glasses with extensive additions of alkali.

4 Conclusions

(1) Mixed α–β-sialons prepared from the UBE Si_3N_4 powder have much higher α/β ratios than the same samples prepared from the Starck powder.

(2) As a consequence of (1), the mixed α–β-sialons prepared from the UBE powder are harder than those prepared from the Starck powder. The K_{IC} values of the former are none the less at least as good as those of the latter. However, the samples with the highest content of α-phase prepared from the UBE powder did not reach acceptable densities at 1825°C when a mixture of Y_2O_3/Nd_2O_3 or pure Nd_2O_3 was used as sintering aid.

(3) The oxidation resistance of mixed α–β-sialons sintered with additions of Y_2O_3 and/or Nd_2O_3 increases with increasing α/β ratio and decreases with decreasing Y_2O_3/Nd_2O_3 ratio. The difference in oxidation resistance between materials sintered with pure Y_2O_3 and pure Nd_2O_3 is considerable.

(4) The lack of smoothness of most oxidation curves makes unambiguous judgement about the oxidation kinetics difficult. The sudden increases in oxidation rates exhibited by most curves are probably due to bursting nitrogen bubbles.

(5) For the two samples that yielded good oxidation data, it seems possible to interpret the TG curves with the new rate law:

$$(\Delta w/A_0) = a \arctan \sqrt{(bt)} + c\sqrt{t}$$

Table 4. The parabolic rate constant K_p and the cross-sectional fraction f for β- and mixed α–β-sialons, oxidized at 1350°C in dry oxygen for 20 h

	Sample								
	A1	*A2*	*A3*	*B1*	*B2*	*B3*	*C1*	*C2*	*C3*
$K_p \times 10^{-4}$ ($mg^2 cm^{-4} s^{-1}$)	1.41	3.66	5.82	—	3.57	3.43	0.291	—	2.29
f	0.35	0.65	0.57	—	0.50	0.42	0.13	—	—

Acknowledgements

This work has been financially supported by the Swedish Board for Technical Development and by AB Sandvik Hard Materials in Stockholm.

References

1. Ekström, T., Käll, P. O., Nygren, M. & Olsson, P. O., Mixed α- and β-(Si–Al–O–N) materials with yttria and neodymia additions. *Mater. Sci. Eng.*, **A105/106** (1988) 161.
2. Käll, P. O. & Ekström, T., Sialon ceramics made with mixtures of Y_2O_3–Nd_2O_3 as sintering aids. *J. Eur. Ceram. Soc.*, **6** (1990) 119.
3. Käll, P. O. & Ekström, T., Phase composition and mechanical properties of HIP-sintered Y/Nd-sialon ceramics. In *Proc. 11th Riso Int. Symp. Metallurgy and Materials Science*, ed. J. J. Bentzen *et al.* Roskilde, Denmark, 1990, p. 383.
4. Persson, J., Käll, P. O. & Nygren, M., Interpretation of the parabolic and non-parabolic oxidation behaviour of Si_2N_2O. *J. Am. Ceram. Soc.*, **75** (1992) 3377.
5. Singhal, S. C. & Lange, F. F., Oxidation behaviour of sialons. *J. Am. Ceram. Soc.*, **60** (1977) 190.
6. Schlichting, J. & Gauckler, L. J., Oxidation of some β-Si_3N_4 materials. *Powder Metall. Int.*, **9** (1977) 36.
7. Lewis, M. H. & Barnard, P., Oxidation mechanisms in Si–Al–O–N ceramics. *J. Mater. Sci.*, **15** (1980) 443.
8. Babini, G. N., Bellosi, A. & Vincenzini, P., A diffusion model for the oxidation of hot-pressed Si_3N_4–Y_2O_3–SiO_2 materials and factors influencing structural evolution in the oxide of hot-pressed Si_3N_4–Y_2O_3–SiO_2 materials. *J. Mater. Sci.*, **19** (1984) 1029, 3487.
9. Patel, J. K. & Thompson, D. P., The low-temperature oxidation problem in yttria-densified silicon nitride ceramics. *Brit. Ceram. Trans. J.*, **87** (1988) 70.
10. Clarke, D. R. & Lange, F. F., Oxidation of Si_3N_4 alloys: Relation to phase equilibria in the system Si_3N_4–SiO_2–MgO. *J. Am. Ceram. Soc.*, **63** (1980) 586.
11. O'Meara, C., Nilsson, P. H. M. & Dunlop, G. L., Oxidation of high-performance ceramics based upon β-Si_3N_4. *Metals Forum*, **8** (1985) 194.
12. Persson, J. & Nygren, M., Oxidation studies of β-sialons. In *Proc. 11th Riso Int. Symp. Metallurgy and Materials Science*, ed. J. J. Bentzen *et al.* Roskilde, Denmark, 1990, p. 451.
13. Persson, J., Käll, P. O. & Nygren, M., A new approach to the interpretation of the oxidation processes in Si_2N_2O-based ceramics. In *Proc. Irish Materials Forum Conference*, ed. S. Hampshire. 1991 and M. Buggy, Trans Tech Publications, Aedermansdorf, 1992, p. 49.
14. Anstis, G. R., Chantikul, P., Lawn, B. R. & Marshall, D. B., A critical evaluation of indentation techniques for measuring fracture toughness: I, Direct crack measurements. *J. Am. Ceram. Soc.*, **64** (1981) 533.
15. Ekström, T., Käll, P. O., Nygren, M. & Olsson, P. O., Dense single-phase β-sialon ceramics by glass-encapsulated hot isostatic pressing. *J. Mater. Sci.*, **24** (1989) 1853.
16. Käll, P. O., Quantitative phase analysis of Si_3N_4-based materials. *Chem. Scr.*, **28** (1988) 439.
17. Huang, Z. K., Tien, T. Y. & Yen, T. S., Subsolidus phase relationships in the Si_3N_4–AlN–rare-earth oxide systems. *J. Am. Ceram. Soc.*, **69** (1986) C-241.
18. Greskovich, C. & Gazza, G. E., Hardness of dense α- and β-Si_3N_4 ceramics. *J. Mat. Sci. Lett.*, **4** (1985) 195.
19. Ekström, T., Effect of composition, phase content and microstructure on the performance of yttrium Si–Al–O–N ceramics. *Mater. Sci. Eng.*, **A109** (1989) 341.
20. Burström, M., Adlerborn, J. & Hermansson, L., High temperature behaviour of HIPed silicon nitride materials evaluated by the STSR-test. In *Proc. Int. Conf. Hot Isostatic Pressing*, ed. T. Garvare. CENTEK, Luleå, Sweden, 1988, p. 383.
21. Tanaka, I., Pezzotti, G., Okamoto, T. & Miyamoto, Y., Dense silicon nitride without additives; Sintering and high-temperature behaviours. *Ceram. Eng. Sci. Proc.*, **10** (1989) 817.
22. Mieskowski, D. M. & Sanders, W. A., Oxidation of silicon nitride sintered with rare-earth oxide additions. *J. Am. Ceram. Soc.*, **68** (1985) C-160.
23. Schlichting, J., Oxidation and hot corrosion behaviour of Si_3N_4 and SiAlON. In *Nitrogen Ceramics*, ed. F. L. Riley. Noordhoff, Leyden, 1977, p. 627.
24. Babini, G. N. & Vincenzini, P., Oxidation kinetics of hot-pressed silicon nitride. In *Progress in Nitrogen Ceramics*, ed. F. L. Riley. Martinus Nijhoff, The Hague, 1983, p. 427.
25. Pomeroy, M. & Hampshire, S., Oxidation processes in silicon-nitride-based ceramics. *Mater. Sci. Eng.*, **A109** (1989) 389.
26. Muehlenbachs, K. & Schaeffer, H. A., Oxygen diffusion in vitreous silica—Utilization of natural isotopic abundances. *Canadian Mineralogist*, **15** (1977) 179.
27. Schaeffer, H. A., Structure–property relationships of the vitreous state. In *Progress in Nitrogen Ceramics*, ed. F. L. Riley. Martinus Nijhoff, The Hague, 1983, p. 303.